The role of Asn-212 in the catalytic mechanism of human endonuclease APE1: Stopped-flow kinetic study of incision activity on a natural AP site and a tetrahydrofuran analogue

ARTICLE *in* DNA REPAIR · JULY 2014

Impact Factor: 3.11 · DOI: 10.1016/j.dnarep.2014.06.008 · Source: PubMed

4 AUTHORS, INCLUDING:

Alexander A Lomzov
Institute of Chemical Biology and Fundame…
28 PUBLICATIONS **94** CITATIONS
SEE PROFILE

Olga S Fedorova
Institute of Chemical Biology and Fundame…
125 PUBLICATIONS **1,075** CITATIONS
SEE PROFILE

DNA Repair 21 (2014) 43–54

Contents lists available at ScienceDirect

DNA Repair

journal homepage: www.elsevier.com/locate/dnarepair

The role of Asn-212 in the catalytic mechanism of human endonuclease APE1: Stopped-flow kinetic study of incision activity on a natural AP site and a tetrahydrofuran analogue

Lyubov Yu. Kanazhevskaya[a,b], Vladimir V. Koval[a,b], Alexander A. Lomzov[a,b], Olga S. Fedorova[a,b,*]

[a] Institute of Chemical Biology & Fundamental Medicine, Siberian Branch of the Russian Academy of Sciences, Lavrentyev Ave., 8, Novosibirsk 630090, Russia
[b] Novosibirsk State University, Pirogova St., 2, Novosibirsk 630090, Russia

ARTICLE INFO

Article history:
Received 27 March 2014
Received in revised form 18 June 2014
Accepted 19 June 2014

Keywords:
Base excision repair
APE1
Abasic site
Stopped-flow method
2-Aminopurine
Pre-steady-state kinetics
MD simulations

ABSTRACT

Mammalian AP endonuclease 1 is a pivotal enzyme of the base excision repair pathway acting on apurinic/apyrimidinic sites. Previous structural and biochemical studies showed that the conserved Asn-212 residue is important for the enzymatic activity of APE1. Here, we report a comprehensive pre-steady-state kinetic analysis of two APE1 mutants, each containing amino acid substitutions at position 212, to ascertain the role of Asn-212 in individual steps of the APE1 catalytic mechanism. We applied the stopped-flow technique for detection of conformational transitions in the mutant proteins and DNA substrates during the catalytic cycle, using fluorophores that are sensitive to the micro-environment. Our data indicate that Asn-212 substitution by Asp reduces the rate of the incision step by ~550-fold, while Ala substitution results in ~70,000-fold decrease. Analysis of the binding steps revealed that both mutants continued to rapidly and efficiently bind to abasic DNA containing the natural AP site or its tetrahydrofuran analogue (F). Moreover, transient kinetic analysis showed that N212A APE1 possessed a higher binding rate and a higher affinity for specific substrates compared to N212D APE1. Molecular dynamics (MD) simulation revealed a significant dislocation of the key catalytic residues of both mutant proteins relative to wild-type APE1. The analysis of the model structure of N212D APE1 provides evidence for alternate hydrogen bonding between Asn-212 and Asp-210 residues, whereas N212A possesses an extended active site pocket due to Asn removal. Taken together, these biochemical and MD simulation results indicate that Asn-212 is essential for abasic DNA incision, but is not crucial for effective recognition/binding.

1. Introduction

The human AP endonuclease 1 (APE1) exhibits an endonuclease activity towards apurinic/apyrimidinic (AP) sites during base excision repair (BER). The AP site produced by DNA glycosylase activity at the first step of the BER pathway is subsequently recognized by APE1, which incises the phosphodiester backbone of DNA immediately 5′ to the lesion. The resulting 3′-OH moiety is processed by DNA polymerase β [1,2]. In addition to endonucleolytic activity, APE1 exhibits 3′–5′ exonuclease and 3′-phosphodiesterase activities [3], which play a significant role in 3′-phosphate and 3′-phosphoglycolate removal, also called "blocking" termini [4]. The structure and enzymatic mechanism of APE1 posed major research areas over the past twenty years. The Protein Data Bank [5] contains eight different crystal structures of the APE1 protein on its own, and complexed with either the substrate or product. According to the structure reported by Tainer et al. [6], APE1 inserts loops into both the major and minor DNA grooves, and binds to a flipped-out AP site in a pocket bordered by hydrophobic and aromatic amino acids. It is important that APE1 mainly contacts the damaged strand of the dsDNA. The APE1-bound DNA is substantially distorted in relation to the B-DNA helix. Stabilization of the kinked abasic substrate is mediated by interactions of one of the APE1 α-helixes with the minor groove, and by the insertion of Met-270, Met-271 and Arg-177 through the minor and major

Abbreviations: APE1, AP endonuclease1; WT, wild type; BER, base excision repair; AP, abasic site; F, 2-hydroxymethyl-3-hydroxy-tetrahydrofuran; 2-aPu, 2-aminopurine; ODN, oligodeoxyribonucleotide; MD, molecular dynamics.

* Corresponding author at: Institute of Chemical Biology & Fundamental Medicine, Siberian Branch of the Russian Academy of Sciences, Lavrentyev Ave., 8, Novosibirsk 630090, Russia. Tel.: +7 383 363 51 75; fax: +7 383 363 51 53.
E-mail address: fedorova@niboch.nsc.ru (O.S. Fedorova).

http://dx.doi.org/10.1016/j.dnarep.2014.06.008
1568-7864/

grooves to occupy the place of the flipped-out AP site. An extensive site-directed mutagenesis study of APE1 showed that the side chains of Asn-226, Asn-229 and Arg-177, interacting with two downstream AP-DNA phosphates, provide specific binding to abasic DNA [7]. Finally, the abasic sugar moiety is stabilized within the hydrophobic active site pocket, which includes the side chains of Phe-266, Trp-280 and Leu-282. Formation of the enzyme's catalytically active state principally depends on the presence and location of the Mg^{2+} ion. This is coordinated by oxygen atoms of the 5′-phosphate moiety as well as by Glu-96 and Asp-70 via a water molecule in the first hydration shell of the metal ion. Previous crystallographic and computational studies suggested two alternative reaction mechanisms: one predicts the presence of two metal ions in the APE1 active site for catalysis [8], while the other model suggests that Mg^{2+} moves from the B-site (Asp-210, Asn-212 and His-309) to the A-site (Asp-70 and Glu-96) during the catalytic cycle [9]. However, the recently published high resolution crystal structure of free APE1 with the essential Mg^{2+} cofactor has confirmed the presence of a single metal ion in the A-site, while the B-site is most probably occupied by a water molecule [10]. The authors also suggest that the water molecule, coordinated by Asn-212 and Asp-210 side chains, serves as a nucleophile for phosphodiester bond hydrolysis. This idea is supported by recently published work, which reported the crystal structure of an APE1-product complex [11]. Additionally, this study provides molecular dynamics simulations of wild type APE1 bound to abasic DNA and its important mutants E96A, Y171P, H309A, N212A, D210N and H309N. These findings show that the phosphate intermediate is stabilized by the Mg^{2+} ion, and contacts His-309 and Tyr-171. Meanwhile, the side chains of Asn-212 and Asp-210 coordinate a water molecule, generating a nucleophile for attacking the phosphodiester bond. Several biochemical studies have described the significance of the conserved Asn-212 residue for APE1 catalytic activity. Rothwell et al. [12] published the first paper on Asn-212 mutants, which reported the important function of Asn-212 in AP site recognition/binding, and incision by APE1 enzyme. Further study demonstrated that substitution of Asn-212 with alanine resulted in a 7000-fold decrease in the processing rate of 52-nt F-containing DNA duplexes [11]. Besides its contribution to catalysis, the Asn-212 residue mediates interactions between APE1 and human DNA glycosylase MYH [13]. A recent bioinformatics study identified possible variations in the APE1 gene that may, in some cases, affect the stability and folding of the enzyme [14]. Particularly, N212H and N212K mutations were found to be deleterious to the function of the protein, indicating the crucial role of the Asn-212 residue.

In our previous studies [15–17], the stopped-flow pre-steady-state kinetic analysis, combined with measurements of the protein tryptophan and DNA 2-aminopurine fluorescence, was successfully applied to detect and quantitatively describe conformational transitions of the enzyme–DNA complex corresponding to particular steps of APE1 reaction. As a result, a four-step kinetic mechanism was proposed, which includes two-step binding, an irreversible substrate cleavage step and dissociation of the enzyme–product complex. Here, the same approach was utilized to investigate the role of the Asn-212 residue in specific steps of APE1 catalysis. A detailed transient kinetic analysis of N212D and N212A APE1 mutants was performed to measure the effect of Asn-212 substitutions on the rates of binding and incision of the specific substrates. Our data showed a substantial reduction of the AP-DNA incision rate by N212D APE1, and practically no incision activity for the N212A mutant. Importantly, the N212A mutant possesses a higher binding affinity to specific substrates compared to the mutant with Asn→Asp substitution.

To obtain a greater understanding of the pre-steady-state kinetic data, we performed MD simulations of WT and mutant APE1 in complex with AP- or F-containing DNA substrates. The findings demonstrated a large distortion of the active site geometry of N212D and N212A mutants, resulting from the dislocation of the key amino acid residues. We found that substitution of Asn-212 with Ala leads to the disruption of the hydrogen bonding network between Asn-212, Asp-210, and catalytic water, whereas the presence of carboxylate at position 212 maintains this network, albeit strongly modified. Thus, this combined biochemical and computational study has elucidated Asn-212's role, during the steps of recognition/binding and incision of abasic DNA by APE1, in more detail.

Table 1
Oligodeoxyribonucleotide substrates utilized in this study.

Substrate	Sequence[a]
AP	5′ CTCTCAPCCTTCC 3′ 3′ GAGAGCGGAAGG 5′
F	5′ CTCTCFCCTTCC 3′ 3′ GAGAGCGGAAGG 5′
AP(2-aPu)	5′ CTCTCAP(2-aPu)CTTCC 3′ 3′ GAGAGCCGAAGG 5′
F(2-aPu)	5′ CTCTCF(2-aPu)CTTCC 3′ 3′ GAGAGCCGAAGG 5′

[a] AP, natural abasic site; F, 2-hydroxymethyl-3-hydroxy-tetrahydrofuran; 2-aPu, 2-aminopurine.

2. Materials and methods

2.1. Oligonucleotides

Oligodeoxyribonucleotides (ODNs; Table 1) containing normal DNA bases, deoxyuridine, tetrahydrofuran, and 2-aminopurine were synthesized on an ASM-700 synthesizer (BIOSSET Ltd., Novosibirsk, Russia) using phosphoramidites, purchased from Glen Research (Sterling, VA) and purified by the anion exchange high-performance liquid chromatography (HPLC) on a Nucleosil 100-10 $N(CH_3)_2$ column followed by the reverse-phase HPLC on a Nucleosil 100-10 C_{18} column (both columns from Macherey-Nagel, Düren, Germany). Concentrations of the ODNs were determined from their absorbance at 260 nm. The AP-containing ODN was prepared by incubation of the deoxyuridine-containing ODN (0.1 mmol) for 14 h at 37 °C with 15 U of uracil-DNA glycosylase in 150 μl of 20 mM Tris–HCl (pH 8.0), 1 mM EDTA, 1 mM dithiothreitol (DTT), 0.1 mg/ml bovine serum albumin, as previously described. The reverse phase HPLC on a Nucleosil 100-5 C_{18} column was used to purify the reaction product, which had a shorter retention time than the starting oligonucleotide, using a linear gradient of 0–20% acetonitrile in 0.1 M triethylammonium acetate (pH 7.0). The pooled fractions were concentrated and then converted to the lithium salt form using a Sep-Pak Plus C_{18} cartridge (Waters, Milford, MA, USA). To confirm the presence of the AP site in the ODN after the treatment with uracil-DNA glycosylase, samples were mixed with 10% aqueous piperidine at 95 °C, or annealed to the complementary oligonucleotide and treated with APE1 under the conditions described below. A PAGE analysis indicated that in both cases the material was cleaved to two shorter oligonucleotides. The purity, homogeneity, and integrity of each ODN were proved by MALDI-TOF mass spectroscopy and assessed by 20% PAGE after staining with Stains-All (Sigma–Aldrich, St. Louis, MO). When needed, the modified DNA strands were ^{32}P-labelled using [γ-^{32}P]-ATP and bacteriophage T4 polynucleotide kinase (SibEnzyme, Russia) according to the manufacturer's protocol, and purified by 20% denaturing PAGE. ODN duplexes were prepared by annealing the modified and complementary strands in a molar ratio of 1:1. Under the conditions of stopped-flow experiments with a high Mg^{2+} concentration (see below), the predicted equilibrium constant of the duplex formation is about $1 \times 10^9\ M^{-1}$, suggesting that nearly 100% of the oligonucleotides are in the double helix form [18–20].

2.2. Site-directed mutagenesis

The desired mutations (N212A and N212D) were introduced into the pET11a plasmid carrying a wild-type *ape1* gene using standard protocol from Stratagene. The following oligonucleotides were used for PCR amplification:

5′ primer (N212D) – 5′GGTCAATTTCTTCATGTGCCAC**ATC**GAGGTCTCCACACAGC

3′ primer (N212D) – 5′GCTGTGTGGAGACCTC**GAT**GTGGCACATGAAGAAATTGACC

5′ primer (N212A) – 5′GGTCAATTTCTTCATGTGCCAC**AGC**GAGGTCTCCACACAGC

3′ primer (N212A) – 5′GCTGTGTGGAGACCTC**GCT**GTGGCACATGAAGAAATTGACC

After digestion with Dpn I final PCR products were electroporated into *Escherichia coli* Eco10 cells (Stratagene, La Jolla, CA) using the *E. coli* Pulser (Bio-Rad, CA). The presence of specific mutations was verified by the dye-terminator nucleotide sequencing.

2.3. Expression and purification of APE1 mutant proteins

The proteins were over-expressed in BL21(DE3) pLysS *E. coli* cells and purified as described previously [15]. The purified fraction of the enzyme was dialyzed in 50 mM Tris–HCl (pH 7.5), 100 mM NaCl, 0.1 mM EDTA, 1 mM dithiothreitol, 50% (v/v) glycerol and stored at −80 °C.

2.4. Stopped-flow fluorescence experiments

Stopped-flow fluorescence measurements were carried out using a model SX.18MV stopped-flow spectrometer (Applied Photophysics, UK) fitted with a 150 W Xe arc lamp. The excitation wavelengths were 280 and 310 nm for tryptophan and 2-aminopurine, respectively. The emission of fluorescence was observed through a 320 nm long-pass filter (Schott, Mainz, Germany) for tryptophan residues and a 370 nm long-pass filter (Corion) for 2-aminopurine. Typically, each trace shown is the average of at least five independent trials. All experiments were carried out at 25 °C in a reaction buffer containing 50 mM HEPES–KOH (pH 7.5), 20 mM KCl, 10 mM $MgCl_2$, and 2 mM DTT. The Trp fluorescence changes were observed with the constant enzyme concentration (1.5 μM) and the ODN concentrations varying from 0.5 to 4 μM. During registration of 2-aPu fluorescence the APE1 concentration was varied in 0.5–3.0 μM range, and the ODN's concentration was 1 μM.

2.5. Bleaching of the enzyme fluorescence

To correct the measured data for bleaching, the fluorescence intensities were recalculated using Eq. (1),

$$F = (F_{obs} - F_b) \times \exp(k_b \times t) + F_b \quad (1)$$

where F is the corrected fluorescence intensity, F_{obs} is the observed fluorescence intensity, F_b is the background fluorescence, and k_b is the coefficient determined for each substrate concentration in experiments with the non-cleavable DNA duplex containing G residue instead of AP or F.

2.6. Pre-steady-state kinetic data analysis

Determination of the mechanism as well as the number of individual reaction steps was implemented as described previously [21,22]. In particular, we fit each fluorescence trace to the sum of exponentials and defined observed rate constants k_i^* of each phase:

$$F = a_1 \exp(-k_1^* t) + a_2(1 - \exp(-k_2^* t)) + C \quad (2)$$

$$E + S \underset{k_{-1}}{\overset{k_1}{\rightleftharpoons}} ES \underset{k_{-2}}{\overset{k_2}{\rightleftharpoons}} (ES)' \xrightarrow{k_3} EP \overset{K_d}{\rightleftharpoons} E + P$$

Scheme 1. The kinetic mechanism for N212D and N212A APE1 derived from global analysis of the stopped-flow fluorescence data. E, APE1; S, free DNA substrate; ES, bimolecular encounter complex; ES′, subsequent state of the APE1-DNA pre-catalytic complex; EP, complex of APE1 with the DNA product; P, product of the substrate incision. Rate constants k_1 and k_2 characterize the forward direction, whereas k_{-1} and k_{-2} are the rate constants for reverse reactions; k_3 corresponds to the irreversible chemical step. K_d is an equilibrium dissociation constant for EP complex decay.

F is the fluorescence intensity at any reaction time t; a_1, a_2 are the amplitudes; k_1^*, k_2^* are the observed rate constants. Values of the obtained rate constants were plotted versus DNA or enzyme concentrations in order to estimate the maximum observed rate and y-intercept. The results were subsequently used as initial values in a global analysis. A global non-linear least-squares fitting was performed using the DynaFit software (BioKin, Pullman, WA) [23]. Differential equations were written for each species in the mechanisms described by Scheme 1. The stopped-flow Trp fluorescence traces were directly fitted by expressing the corrected fluorescence intensity (F_c) at any reaction time t as the sum of the background fluorescence (F_b) and the fluorescence intensities of each protein species:

$$F_c = F_b + \sum_{i=0}^{n} F_i(t) \quad (3)$$

$F_i(t) = f_i(E_i(t))$, f_i is the coefficient of specific fluorescence for each discernible APE1 conformer, and ($E_i(t)$) is the concentration of the conformer at any given time t ($i = 0$ relates to the free protein, and $i > 0$, to the protein–DNA complexes). These specific fluorescence coefficients describe only the part of fluorescence that changes due to DNA binding. Similar fitting procedures were carried out for 2-aPu fluorescence traces with the difference that fluorescently discernible transient states corresponded to DNA species. The minimal nature of the reaction schemes was confirmed using a "scree test" [22]. Errors in all rate constant values measured by the stopped-flow assay did not exceed 10%.

2.7. Steady-state fluorescence measurements

Proceeding of the reaction under steady-state conditions was monitored using 2-aPu fluorescence of DNA-substrates. The experiments were performed on a Cary Eclipse fluorescence spectrophotometer (Varian, Australia). All the reaction conditions including DNA and protein concentrations, temperature and the buffer were completely similar to stopped-flow experiments. To initiate the process 40 μl of 1.5 μM enzyme and 40 μl of the substrate were rapidly mixed in a fluorescence cuvette. The first time point of each fluorescent trace was 30 s caused by the need of hand mixing of reagents. The 2-aPu fluorescence change was monitored over time with excitation wavelength set at 310 nm and emission at 370 nm. The quantitative analysis of the series of kinetic curves was the same as for pre-steady-state stopped-flow kinetics using the DynaFit software.

2.8. Cleavage time course analysis

The damaged DNA strands were 5′-labelled with ^{32}P and annealed to the complementary strand. To start the reaction 1.5 μM substrates were mixed with 1.5 μM enzyme in the reaction buffer containing 50 mM HEPES–KOH (pH 7.5), 20 mM KCl, 10 mM $MgCl_2$, and 2 mM DTT. The reaction was terminated at required time points by the addition of a loading dye solution containing 7 M urea.

Aliquots were then analyzed by 20% denaturing PAGE, the gels were imaged by autoradiography and quantified by scanning densitometry using Gel-Pro Analyzer 4.0 software (Media Cybernetics, Silver Spring, MD). The data were analyzed with the assumption that a catalytic rate constant, denoted as k_{inc}^{PAGE}, is a ratio of initial velocity V_0 to the equilibrium concentration of the pre-catalytic complex [ES′] using the following equation:

$$k_{inc}^{PAGE} = 2V_0 \left(e_0 + s_0 + \frac{1}{K_a} + \sqrt{\left(e_0 + s_0 + \frac{1}{K_a} \right)^2 - 4e_0 s_0} \right)^{-1} \quad (4)$$

where V_0 is the initial velocity derived from the slope angle of the linear part of the PAGE time course; e_0 and s_0 are total concentrations of the enzyme and DNA; K_a is an equilibrium association constant derived from a quantitative analysis of the appropriate stopped-flow data.

2.9. Molecular dynamic simulations

The atomic structure of human APE1 (Protein Data Bank entry 1DEW) containing a 15-mer DNA duplex was taken for modelling. Amino acid residues 1–40 were absent in the initial structure, and an MD simulation was carried out as is. It should be noted that this domain is located on the other side of APE1 spatial structure from the DNA binding site. The N212D and N212A mutations were inserted by manual editing the PDB file. The DNA duplex was manually truncated to 12-mer and edited so that it contained the 2-aminopurine residue 3′ to the F site. The Mg^{2+} ion was placed to the PDB file according to previously published data [11,24]. The final refinement was done by 500 ps of simulated annealing using the AMBER 12 molecular modelling suite [25]. The mutant structures were finally validated using the PDB AmberTools 13 validation module [26]. AMBER force field parameters for the 5′-phosphate residue of the 2-aPu base were taken from the AMBER parameter database [27]. The catalytically important His-309 residue was set as protonated. A 10 ns molecular dynamics simulation was performed using the AMBER 12 MD software with GPU accelerated code [26,28,29]. We employed the ff99SB force field and the analytical implicit solvent model with an integration time step of 1 fs. The system was gradually heated from 1.2 K to 300 K over 2500 ps and equilibrated at the room temperature. A classic molecular dynamics trajectory was generated in the NTV ensemble with harmonic restraints of 0.001 kcal/Å^2 for the protein atoms, 0.25 kcal/Å^2 for atoms of the terminal nucleotides, and 0.0025 kcal/Å^2 for the rest of the DNA atoms. Coordinates of each atom of the system (snapshots) were saved every 1 ps. We apply the UCSF Chimera package to generate a molecular graphics, MD movies and its analysis [30]. The structures were visualized using the PyMOL molecular graphics system (Schrödinger, LLC, New York).

3. Results

It is known from literature that human APE1 protein binds to an incised product DNA of 30 nt and longer with the affinity very close to that of non-incised DNA substrate [31,32]. In some cases, the step of incised product release is rate-limiting [33–35]. To detect of conformational changes corresponding to steps of specific binding and incised product release during the transient kinetic analysis, we designed 12 bp abasic DNA duplexes. The structures and short names of oligodeoxyribonucleotides (ODNs) that serve as specific substrates for APE1 are presented in Table 1. As shown in our previous study, these complementary oligodeoxyribonucleotides exist in a duplex form under experimental conditions does not show appreciable end effects [16]. 2-Hydroxymethyl-3-hydroxytetrahydrofuran (denoted as “F”) is a chemically stable analogue of the natural AP site, which is not susceptible to β-elimination. ODNs containing the F-lesion are recognized and processed as specific substrates by AP endonucleases [36]. It was previously found that the fluorescent base 2-aminopurine, located upstream (5′ to the AP site), impeded the incision of the damaged strand by WT APE1, while a downstream (3′ to the AP site) 2-aPu had no influence on the reaction execution [16]. For this reason, in the present study, we inserted the 2-aPu probe 3′ to the AP site in ODN's sequences to detect conformational transitions of DNA substrates.

3.1. Kinetics of abasic DNA incision by N212D APE1

First, the pre-steady-state kinetics of abasic DNA incision by N212D APE1 was measured. The series of stopped-flow fluorescence curves collected under single turnover conditions, over the range of either substrate or enzyme concentrations, are presented in Fig. 1.

Conformational changes within the protein molecule were monitored by Trp fluorescence, from 1 ms to 2000 s, after quick reagent mixing (Fig. 1A and B). To observe the conformational transitions of specific substrates during binding and incision by N212D APE1, we measured 2-aPu fluorescence (Fig. 1C and D). Since the fluorescence curves showed both fast and relatively slow phases, data were collected in different time windows. The resulting time courses demonstrated significant conformational changes of the mutant enzyme and the DNA substrates. The traces can be divided into individual phases of the fluorescence growth and decay, which correspond to particular reaction steps. Behaviour of the initial parts of the traces suggests that the catalytic complex formation, between the N212D mutant and AP (or F) substrate, is realized in two steps taking place between 0.01 and 2 s. Since the initial collision complex forms at a very fast rate, the stopped-flow method is able to detect only the end of this process, as expressed by a slight 2-aPu fluorescence increase between 0.001 and 0.05 s (Fig. 1C and D). In the second phase, the quenching of both Trp and 2-aPu fluorescence, suggested that the flipped-out AP site was immersed into the hydrophobic active site pocket. The third phase showed a substantial increase in fluorescence intensity (30–200 s) and was followed by a plateau in the final part of the trace (Fig. 1A–C). In contrast, the final part of fluorescent traces in Fig. 1D demonstrated a little increase of the fluorescent signal, indicating a reduced rate of that conformational change for F(2-aPu) substrate processing. As the fluorescence of Trp and 2-aPu is strongly quenched by DNA bases, it seems likely that the third phase of the curve corresponds to incision of the substrate, followed by release of shortened ODNs from the enzyme's active site. It is important to note that the overall shapes of the fluorescence traces, obtained for N212 APE1, resemble those obtained for WT APE1, although the presence of Asn→Asp substitution reduced the rate of each step of the process [15].

For assigning the kinetic mechanism, the series of kinetic curves obtained at different concentrations of enzyme or/and DNA–substrates were globally fitted, as described in Section 2.6 and in our previous studies [15,16]. The initial estimation of an equilibrium Kd constant was provided by independent fluorescent titration of the mutants with a mixture ODNs representing the incised DNA product (data not shown). The resulting kinetic mechanism outlined in Scheme 1 includes two reversible steps, one irreversible step and the final equilibrium corresponding to decomposition of the enzyme–product complex (EP).

The quality of the fit was estimated by inspection of residuals (Fig. S1 in the Supplementary Material). Table 2 summarizes the forward and reverse rate constants associated to interactions of N212D APE1 with AP- and F-containing DNA duplexes.

As expected, the rate constants of the same steps of Scheme 1, measured by Trp and 2-aPu fluorescence, corresponded to one another. The binding event occurred in two reversible steps

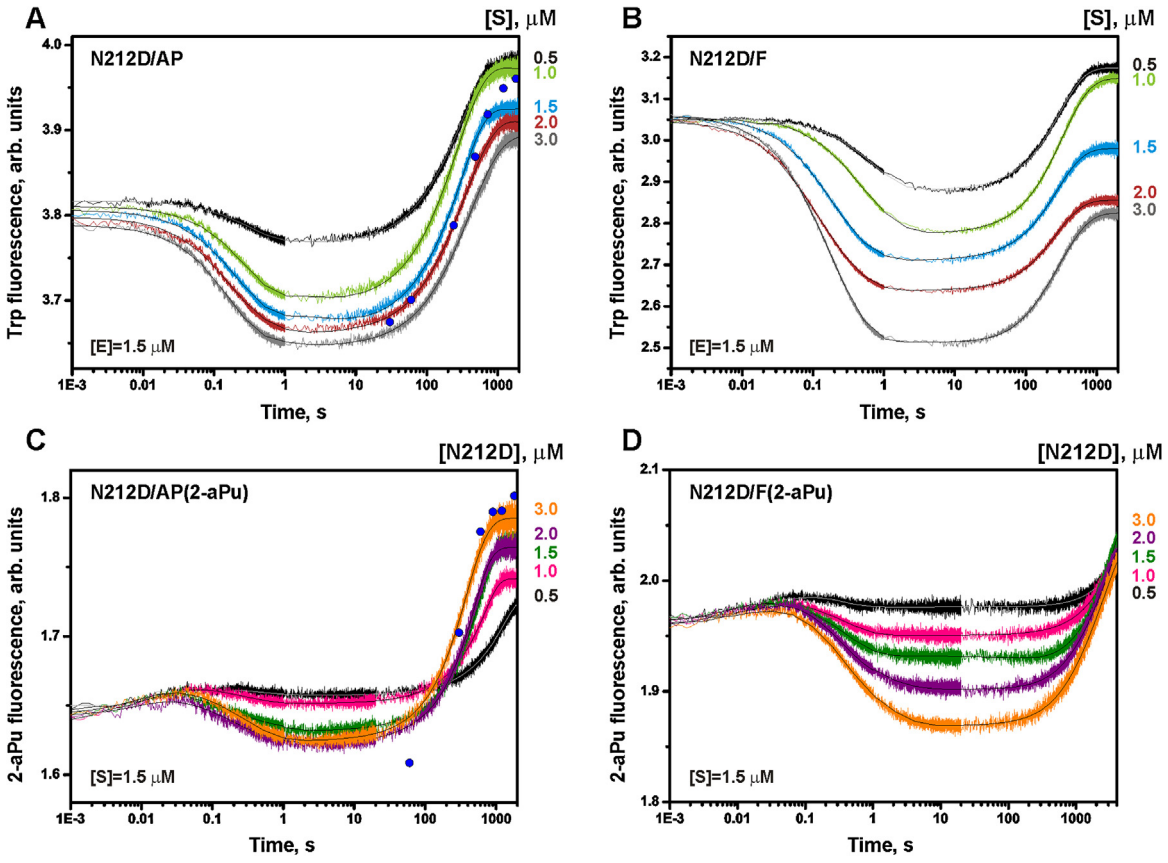

Fig. 1. Changes in the Trp or 2-aPu fluorescence intensity during binding and incision of AP- and F-containing substrates by N212D APE1. (A, B) Time dependencies of conformational transitions within the protein molecule at varied concentrations of abasic DNA are shown. (C, D) Time dependencies of conformational transitions within the DNA substrate at varied concentrations of the enzyme are shown. Jagged traces represent experimental data; smooth curves are the result of global fitting to Scheme 1. Blue circles represent time dependencies of cleaved ODNs accumulation derived from PAGE analysis (A, C). Rate constants derived from global analysis of kinetic data are shown in Table 2. (For interpretation of the references to colour in this figure legend, the reader is referred to the web version of the article.)

was described by equilibrium constants K_1 and K_2. The k_1 and k_{-1} rate constant values were typical for initial non-specific enzyme–substrate interactions. It was observed that K_1 values for AP or F substrate did not depend on the type of fluorophore, while K_2 values measured by 2-aPu fluorescence were 2.5–6-fold higher than these values measured by Trp fluorescence. Apparently, this is associated with the indistinct concentration dependence at the second phase of Trp fluorescence traces in the 0.1–1 s time interval, resulting in low accuracy of determining the K_2 values (Fig. 1A and B). In spite of this difference, the level of (ES)′ complex formation, which can be estimated from the equation $[ES'] \approx K_1 \times K_2 \times C/(1 + K_1 \times C + K_1 \times K_2 \times C)$ (C is the concentration of E or S depending on the type of experiment), varies in the range of 20–30%. The affinity of mutant enzymes to abasic substrates was evaluated using an equilibrium association constant, K_a. Comparing K_a values, the N212D mutant revealed a three times higher affinity to the chemically stable F than to the natural AP site. The K_a^F/K_a^{AP} ratio determined for WT APE1 was 3.2, indicating the agreement between kinetic data for mutant and WT enzymes [15]. The rate constant of the third irreversible step for AP substrate cleavage,

Table 2
Kinetic parameters of N212D APE1 activity on AP- and F-containing substrates, derived from the global fitting to Scheme 1. Errors shown represent a standard deviation of theoretically fitted plots from the stopped-flow curves. Importantly, an actual error value also involves experimental errors (e.g. machine noise, dilution and mixing error), being close to 10%.

Enzyme/substrate	Trp fluorescence			2-aPu fluorescence	
	N212D/AP	N212D/F	WT APE1/AP[b]	N212D/AP(2-aPu)	N212D/F(2-aPu)
k_1, M^{-1} s^{-1}	$(2.3 \pm 0.1) \times 10^6$	$(5.4 \pm 0.2) \times 10^6$	$(8.9 \pm 0.5) \times 10^7$	$(2.2 \pm 0.3) \times 10^7$	$(7.8 \pm 0.1) \times 10^7$
k_{-1}, s^{-1}	7.6 ± 0.4	4.9 ± 0.1	6.0 ± 0.7	62 ± 3	61 ± 5
K_1, M^{-1}	$(3.0 \pm 0.3) \times 10^5$	$(1.1 \pm 0.1) \times 10^6$	$(1.5 \pm 0.2) \times 10^7$	$(3.6 \pm 0.6) \times 10^5$	$(1.3 \pm 0.1) \times 10^6$
k_2, s^{-1}	6.7 ± 0.3	5.0 ± 0.2	3.2 ± 0.1	4.8 ± 0.3	2.3 ± 0.1
k_{-2}, s^{-1}	2.3 ± 0.1	3.7 ± 0.1	1.8 ± 0.1	0.68 ± 0.01	0.35 ± 0.01
K_2	2.9 ± 0.2	1.4 ± 0.1	1.8 ± 0.2	7.1 ± 0.5	6.6 ± 0.5
k_3, s^{-1}	0.0058 ± 0.0004	0.0049 ± 0.0003	3.20 ± 0.06	0.0050 ± 0.0004	ND
K_d, M	$(1.2 \pm 0.1) \times 10^{-6}$	$(3.3 \pm 0.3) \times 10^{-6}$	$(1.0 \pm 0.1) \times 10^{-6}$	$(2.7 \pm 0.2) \times 10^{-6}$	ND
K_a, M^{-1} [a]	$(6.8 \pm 1.4) \times 10^5$	$(1.5 \pm 0.2) \times 10^6$	$(4.1 \pm 0.5) \times 10^7$	$(2.5 \pm 0.6) \times 10^6$	$(8.3 \pm 1.3) \times 10^6$

[a] The equilibrium association constant was calculated from the equation $K_a = K_1 \times K_2$, where $K_i = (k_i/k_{-i})$.
[b] Data from Kanazhevskaya et al. [15].

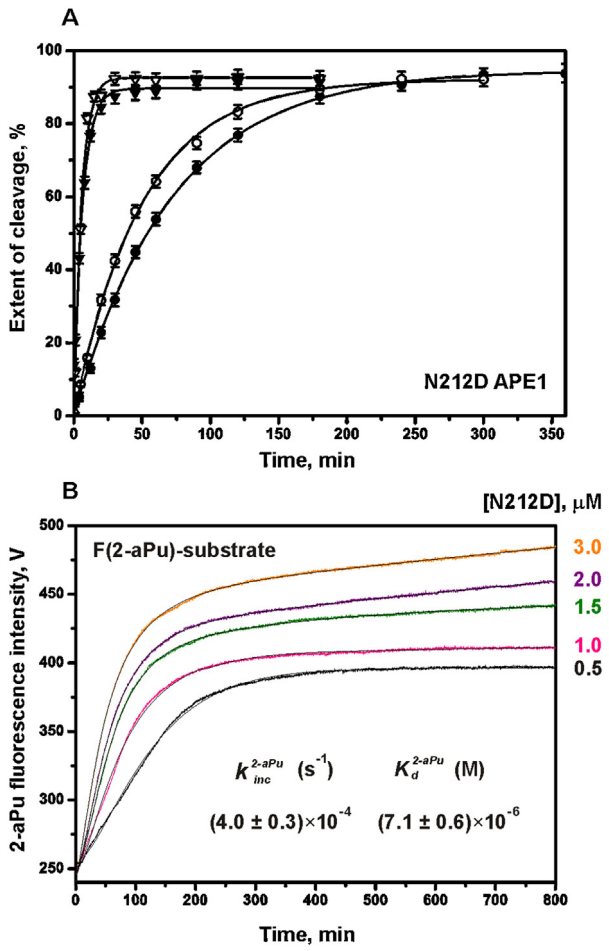

Fig. 2. (A) Cleavage of ^{32}P-labelled DNA substrates by N212D APE1. Time courses of the cleaved product accumulation for AP- (▼), F- (●), AP(2-aPu)- (▽) and F(2-aPu)- (○) substrates were measured using the chemical quench assay. The resultant concentration of the enzyme and substrates was 1.5 μM. The reaction conditions were identical to stopped-flow experiments. Error bars reflect the standard error of the mean from three independent experiments. Analysis of the experimental points using Eq. (4) (see Section 2.9) provided the cleavage rate constant, k_{inc}^{PAGE}, shown in Table 3. (B) Steady-state fluorescence measurement of the F(2-aPu) substrate cleavage by various concentrations of N212D APE1. Values of k_{inc}^{2-aPu} and K_d^{2-aPu} constants were derived by the global data fitting to Scheme 2.

k_3^{AP}, had a value of 0.0058 ± 0.0004 s^{-1}, which was 550 times lower than that of WT APE1. A similar value of k_3^{F} = 0.0049 ± 0.0003 s^{-1} was found for F substrate incision by N212D APE1. Values of the dissociation constant K_d, which described the fourth equilibrium of the mechanism, did not vary much between substrate types, and were close to 2.5 μM. Interpreting the pre-steady-state kinetic data suggests the existence of a stable (EP) complex between N212D APE1 and AP-containing DNA, impeding the release of reaction products from the mutant active site.

To measure the rate of substrate incision using an independent approach, we performed a chemical quench experiment with ^{32}P-labelled substrates followed by PAGE analysis of the reaction products. Fig. 2A represents the kinetics of ODN product accumulation when interacting with N212D APE1. To compare stopped-flow and chemical quench data we superimposed PAGE analysis results for AP and AP(2-aPu) substrates (blue circles) and the appropriate stopped-flow fluorescence traces (see Fig. 1A and C). It is obvious that accumulation of labelled products overlaps with the phase of Trp and 2-aPu fluorescence growth, which corresponds to the third irreversible step of Scheme 1. Fitting the PAGE time courses to Eq. (4) allows estimation of the incision rate constant k_{inc}^{PAGE} for each

Table 3
Rate constants of specific substrates incision by APE1 derived from PAGE analysis using Eq. (4). The error of the estimated values did not exceed 25%.

	Substrate	N212D APE1	N212A APE1
k_{inc}^{PAGE}	AP	0.0028 s^{-1}	4.4 × 10^{-5} s^{-1}
	F	3.0 × 10^{-4} s^{-1}	2.3 × 10^{-5} s^{-1}
	AP(2-aPu)	0.0024 s^{-1}	4.1 × 10^{-5} s^{-1}
	F(2-aPu)	1.8 × 10^{-4} s^{-1}	1.4 × 10^{-5} s^{-1}

$$E + S \underset{}{\overset{K_a}{\rightleftharpoons}} (ES)' \xrightarrow{k_{inc}^{2\text{-}aPu}} EP \overset{K_d^{2\text{-}aPu}}{\rightleftharpoons} E + P$$

Scheme 2.

substrate. The values of the K_a constant, in this analysis, were calculated from global analysis of the stopped-flow data. The estimated values of k_{inc}^{PAGE} for AP and F substrates, presented in Table 3, are 0.0028 s^{-1} and 3.0 × 10^{-4} s^{-1}, respectively.

Fig. 1D represents the stopped-flow kinetics of interactions of N212D APE1 with F-containing DNA measured by 2-aPu fluorescence. Interestingly, the fluorescent signal does not attain a maximum value during measurement, and the last fluorescently discernible step is a continuous growth from 50 s to 4000 s. Thus, it is impossible to derive the values of k_3 and K_d constants by global data fitting to Scheme 1. The rate of F(2-aPu) substrate cleavage was measured by routine fluorimetry, which included measuring the 2-aPu fluorescence in the 0.5–800 min time interval after manually mixing the enzyme and DNA solutions (Fig. 2B). The resulting steady-state kinetic curves demonstrated a slow accumulation of incised product (P) and its complex with enzyme (EP). This approach allowed measuring the hyperbolic increase in the 2-aPu fluorescence indicating DNA strand cleavage, followed by fluorophore translocation into the solution. For this reason, the set of curves was fitted to a simplified Scheme 2, where the first equilibrium consolidated the two binding steps of Scheme 1.

As a result, the incision rate constant, k_{inc}^{2-aPu}, of (4.0 ± 0.3) × 10^{-4} s^{-1} was found. This value is two times higher than the rate constant derived from direct PAGE analysis for the same substrate (see Table 3). The last equilibrium of Scheme 2 represented the mutant-product (EP) complex decomposition governed by a dissociation constant, K_d^{2-aPu}, of (7.1 ± 0.6) × 10^{-6} M. This value together with K_d for F substrate obtained from the stopped-flow data suggests that N212D APE1 has a lower affinity for F-containing ODN products as compared to AP-containing products.

3.2. Pre-steady-state kinetics of interactions between N212A APE1 and abasic DNA

To better understand the role of Asn-212 in APE1 active site functioning, we further investigated the activity of N212A mutant lacking the amide or carboxyl moiety in position 212. Stopped-flow traces of Trp and 2-aPu fluorescence intensity were measured at mutant and DNA concentrations ranging from 0.5 to 4.0 μM (Fig. 3). During N212A APE1 interactions with either the natural AP site or F, the fast phase of Trp fluorescence decrease was detected within 1–200 ms, which most likely corresponded to the substrate binding steps (Fig. 3A and B).

In the next phase, the kinetic curves exhibited a moderate fluorescence increase, followed by an indistinct plateau between 150 and 1500 s. The set of kinetic curves obtained for binding and incision of abasic DNA by N212A mutant fit well with the four step kinetic mechanism of Scheme 1, as in the case of N212D APE1. The results of global fitting are summarized in Table 4.

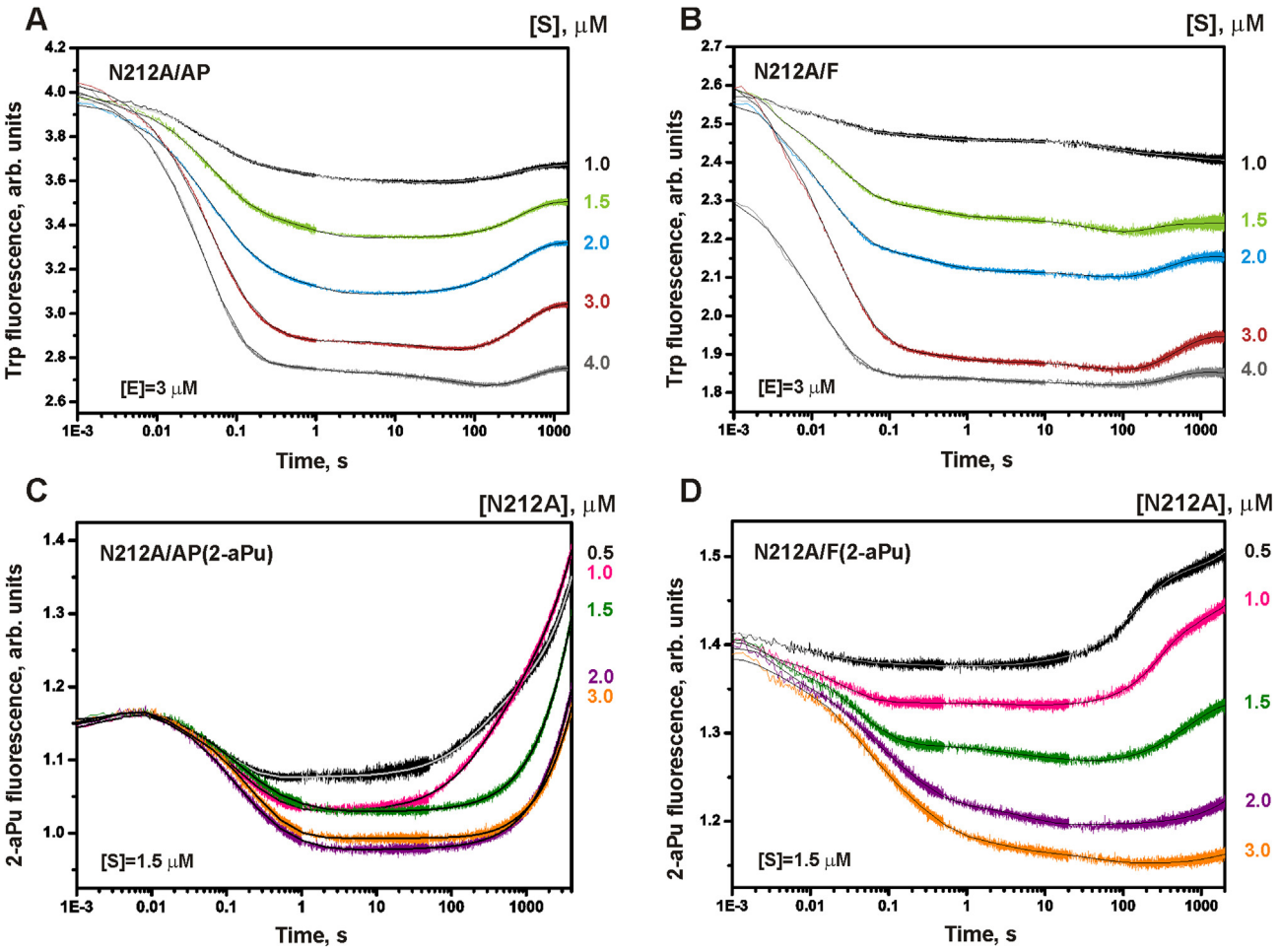

Fig. 3. Changes in the Trp or 2-aPu fluorescence intensity during binding and incision of AP- and F-containing substrates by N212A APE1. (A, B) Time dependencies of conformational transitions within the protein molecule at varied concentrations of abasic DNA are shown. (C, D) Time dependencies of conformational transitions within the DNA substrate at varied concentrations of the enzyme are shown. Jagged traces represent experimental data; smooth curves are the result of global fitting to Scheme 1. Rate constants derived from global analysis of kinetic data are shown in Table 3.

The values of forward rate constants k_1 and k_2, which characterized N212A APE1 binding to AP and F substrates, were distinctly higher than that of the N212D mutant. Indeed, in terms of the rate constant k_2, the mutant APE1 containing the Asn→Ala substitution binds F substrate three times faster than APE1 with Asn→Asp substitution. Thus, the values of the equilibrium association constants $K_a^{N212A/AP} = (2.5 \pm 0.3) \times 10^6\ M^{-1}$ and $K_a^{N212A/F} = (4.9 \pm 0.4) \times 10^6\ M^{-1}$ are, on average, three and a half times higher as compared to N212D APE1. The conformational transitions observed as a weak increase in Trp fluorescence in Fig. 3A and B might correspond to substrate incision in the third step of Scheme 1. The global analysis of N212A mutant kinetics yielded rate constants, k_3, of $0.0023 \pm 0.0001\ s^{-1}$ and $(4.5 \pm 0.2) \times 10^{-4}\ s^{-1}$ for AP and F substrate, respectively. To ascertain the nature of this conformational transition, we measured the reaction product accumulation using the chemical quench assay (Fig. 4A). Using PAGE analysis we found that a 33 min treatment with N212A APE1 (that matches a time window of stopped-flow traces) resulted in 20% incision of AP substrate and 10% of F substrate at the rates of $4.4 \times 10^{-5}\ s^{-1}$ and $2.3 \times 10^{-5}\ s^{-1}$, respectively. Therefore, we

Table 4
Kinetic parameters of N212A APE1 activity on AP- and F-containing substrates derived from the global fitting to Scheme 1. Errors shown represent a standard deviation of theoretically fitted plots from the stopped-flow curves. Importantly, the actual error value also involves experimental errors (e.g. machine noise, dilution and mixing error), being close to 10%.

Enzyme/substrate	Trp fluorescence		2-aPu fluorescence	
	N212A/AP	N212A/F	N212A/AP(2-aPu)	N212A/F(2-aPu)
k_1, $M^{-1}\ s^{-1}$	$(3.2 \pm 0.1) \times 10^7$	$(7.4 \pm 1.0) \times 10^7$	$(2.1 \pm 0.1) \times 10^7$	$(3.1 \pm 0.2) \times 10^7$
k_{-1}, s^{-1}	35 ± 1	28 ± 2	15 ± 0.5	26 ± 0.1
K_1, M^{-1}	$(9.1 \pm 0.5) \times 10^5$	$(2.6 \pm 0.5) \times 10^6$	$(1.4 \pm 0.1) \times 10^6$	$(1.2 \pm 0.1) \times 10^6$
k_2, s^{-1}	13.0 ± 0.7	18 ± 1	7.8 ± 0.4	6.6 ± 0.3
k_{-2}, s^{-1}	4.6 ± 0.2	9.7 ± 0.3	0.78 ± 0.04	6.1 ± 0.2
K_2	2.8 ± 0.3	1.9 ± 0.2	10 ± 1.0	1.1 ± 0.1
k_3, s^{-1}	0.0023 ± 0.0001	$(4.5 \pm 0.2) \times 10^{-4}$	ND	ND
K_d, M	$(3.6 \pm 0.4) \times 10^{-6}$	$(0.7 \pm 0.1) \times 10^{-6}$	ND	ND
K_a, M^{-1}	$(2.5 \pm 0.4) \times 10^6$	$(4.9 \pm 1.4) \times 10^6$	$(1.5 \pm 0.2) \times 10^7$	$(1.3 \pm 0.2) \times 10^6$

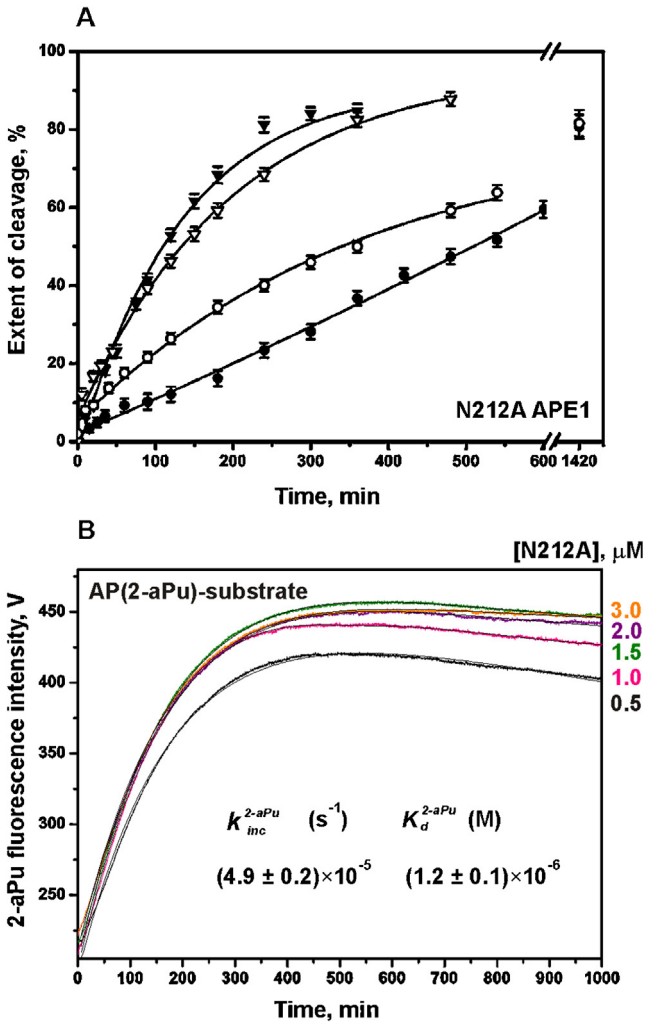

Fig. 4. (A) Cleavage of ^{32}P-labelled DNA substrates by N212A APE1. Time courses of the cleaved product accumulation for AP- (▼), F- (●), AP(2-aPu)- (▽) and F(2-aPu)- (○) substrates were measured using the chemical quench assay. The resultant concentrations of the mutant and substrates were 2 μM for pairs N212A–AP substrate, N212A–F substrate and 1.5 μM for pairs N212A–AP(2-aPu) substrate, N212A–F(2-aPu) substrate. Conditions of the reaction were identical to stopped-flow experiments. Error bars reflect the standard error of the mean from three independent experiments. Analysis of the experimental points using Eq. (4) (see Section 2.9) provided the cleavage rate constant, k_{inc}^{PAGE}, shown in Table 3. (B) Steady-state fluorescence measurement of the AP(2-aPu) substrate cleavage by various concentrations of N212A APE1. Values of k_{inc}^{2-aPu} and K_d^{2-aPu} constants were derived by the global data fitting to Scheme 2.

suggest that the Trp fluorescence increase, observed as the third step of the kinetic curves, actually represents the initial stage of the reaction product formation. These findings indicate a 68,000-fold reduction in AP and F substrate processing rate when Asn-212 of native APE1 is substituted with Ala.

Fluorescence traces of DNA substrate dynamics, obtained from the stopped-flow traces of N212A APE1 and AP(2-aPu) substrate interactions, consisted of three phases: a slight growth from 1 to 10 ms, a pronounced decrease from 10 ms to 1 s, and a substantial increase between 150 and 4000 s (Fig. 3C). The third phase of 2-aPu fluorescence traces did not transformed to a hyperbolic form up to 4000 s. Thus, it was impossible to adequately fit this set of time courses to Scheme 1, and to separately determine the values of the k_3 and K_d constants. In the course of quantitative analysis, the fluorescent curves were restricted by 7 s, and then fitted to a "shortened" Scheme 3, which included two binding steps.

$$E + S \underset{k_{-1}}{\overset{k_1}{\rightleftharpoons}} ES \underset{k_{-2}}{\overset{k_2}{\rightleftharpoons}} (ES)'$$

Scheme 3.

The resulting rate constant values of forward and reverse reactions derived from 2-aPu fluorescence traces are close to that of the Trp fluorescence (see 1st and 3rd columns of Table 3), indicating fast and effective binding of specific substrates by N212A APE1. To observe the final reaction steps, the enzyme and the AP(2-aPu) substrate were mixed, and the 2-aPu fluorescence signal was measured up to 1000 min using steady-state fluorescence. The set of kinetic curves presented in Fig. 4B was fitted to the simplified Scheme 2. This gave the rate constant of AP(2-aPu) substrate incision of $(4.9 \pm 0.2) \times 10^{-5}$ s^{-1}, which is in good agreement with the incision rate constant (4.1×10^{-5} s^{-1}) estimated by PAGE analysis (Table 3). In addition, steady-state fluorescence measurements revealed the high affinity of N212A APE1 to the nicked DNA product characterized by the equilibrium dissociation constant, K_d, of $(1.2 \pm 0.1) \times 10^{-6}$ M.

Pre-steady-state kinetics of interactions between the N212A mutant and the F(2-aPu) substrate demonstrated a distinctive behaviour of the conformational transitions (Fig. 3D). The 2-aPu fluorescence time courses did not display the representative increase from 1 to 50 ms, while the process of enzyme–substrate binding was accompanied by an extended multistep decrease of the fluorescence intensity. Visual inspection of kinetic curves suggested the existence of at least three conformational transitions of the DNA substrate upon specific binding to N212A APE1, but amplitudes of the signal were too low for its quantitative analysis. Consequently, data were fitted to the two-step binding Scheme 3 in which an initial non-specific complex (ES) converted to a high-affinity complex (ES)′. The resulting values of forward and reverse rate constants are consistent with those derived from Trp fluorescence measurements. In the case of F(2-aPu) substrate, the slow step corresponding to the initial stage of DNA incision was observed as a moderate growth of 2-aPu fluorescence (from ~150 s), which became biphasic at low enzyme concentrations. This effect may be due to the appearance of small amounts of ODN products in the reaction mixture. On the other hand, the relative stability of the complex (EP) inhibits further product accumulation and release from the mutant active site. An attempt to measure the rate of the incision step by steady-state fluorescence was unsuccessful because the time dependencies did not saturate up to 1200 min during measurement (Fig. S2 in the Supplementary Material). In addition, the concentration dependence of the kinetic curves was not pronounced enough to accurately determine the kinetic parameters. To estimate the rate of F(2-aPu) substrate cleavage by N212A APE1, we analyzed the data obtained by the chemical quenching experiment. The value of incision constant, k_{inc}^{PAGE}, was 1.4×10^{-5} s^{-1}, which is one order of magnitude lower compared to N212D APE1.

3.3. MD simulations of N212A and N212D APE1 structures

To identify the structural changes in the mutant enzymes that lead to reduced catalytic activity, MD simulations of the enzyme complexed with the F(2-aPu) substrate, were undertaken for WT, N212D, and N212A APE1. Simulations at 300 K provided information about the dynamic behaviour of the molecular system. In our molecular modelling, we started with the published crystal structure 1DEW [6]. Fig. 5 represents a general view of the WT APE1–DNA complex and its magnified part representing localization of the key amino acids and the Mg^{2+} ion within the active site.

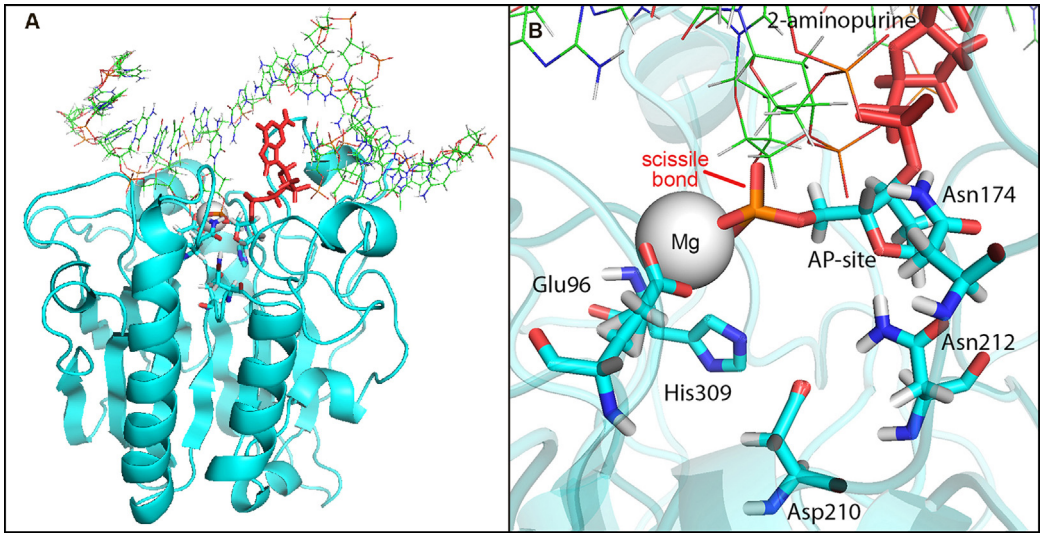

Fig. 5. (A) An overall view of APE1 molecular complex with the DNA duplex. The 2-aPu base is shown in red sticks; F site is shown as a stick model coloured according to the atom type (*cyan*, carbons; *blue*, nitrogens; *red*, oxygens; *brown*, phosphorus atoms). (B) Active site residues localization. Mg^{2+} ion is shown as grey CPK sphere, Glu-96, Asn-174, Asp-210, Asn-212 and His-309 amino acid residues forming the active site are shown in stick models coloured according to the atom type. The rest of the protein is shown as a semitransparent schematic model. The molecular structures were visualized using the PyMOL software package. (For interpretation of the references to colour in this figure legend, the reader is referred to the web version of the article.)

MD movies of 10 ns simulations for three enzyme–substrate complexes are presented in the Supplementary Material (Fig. S3–S5). A significant problem for MD simulation is the correct positioning of the metal ion in the APE1 structure. While editing the PDB file, we placed the Mg^{2+} ion by taking into account the general principles underlying metal ion coordination in proteins and the recently published data [10,11,24]. The resulting structure was subjected to minimization in which the metal ion and amino acids were allowed to adopt an optimal conformation. Following analysis of the movies, we found that all three models were rather stable, and did not show dissociation of enzyme–substrate complexes. During the simulation process mobile domains of the protein generally exposed to solution. The distance between terminal nucleotides of DNA duplexes increased occasionally, which resulted in the destruction of Watson-Crick hydrogen bonds. We should note that the described behaviour of the molecular complex is common in MD simulations. Position of the F site, flipped into the APE1 catalytic pocket, was persistent throughout the MD trajectory. As expected, the 2-aPu fluorescent base formed a mobile mispair with cytosine [37], which was located in close proximity to the abasic site void. Thus, it can be stated that the 2-aPu fluorescence changes detected by the stopped-flow method directly reflect conformational transitions within the enzyme active site. All three models evolved slowly at the initial stage of the run (up to 4–5 ns), and were quite stable after 5 ns as evidenced by two-dimensional RMSD plots (Fig. S6A–C).

MD simulations also showed that the Mg^{2+} ion in WT APE1 lies within 1.9 Å of the Glu-96 carboxylate moiety, 1.87 Å of the Asp-308, and within 1.96 Å of the F site 5′-phosphate (Fig. 5B). The distance between the metal ion and side chains of Asn-212 and Asp-210 was 7.6 Å and 6.6 Å, respectively, suggesting that these amino acids did not participate in the Mg^{2+} coordination. Position of the metal ion was persistent throughout the MD trajectory. The results of MD simulations suggested a direct coordination of Mg^{2+} by the Asp-308 carboxylate (Fig. 6A). In the recently published crystal structure of free APE1 with the Mg^{2+} cofactor Asp-70 was found in the first coordination sphere of the metal ion, whereas Asp-308 participated in the metal coordination through a water molecule [10]. Our results revealed that the side chain of Asp-308 was lying closer to Mg^{2+} than Asp-70, making possible the immediate contact. The finding is in good agreement with the results of a biochemical study, where the WT and D308A APE1 interactions with DNA substrate and product at varying concentration of Mg^{2+} were examined [33]. The computational analysis also shows that the metal ion is hexagonally coordinated by carboxylate groups of Asp-308 and Glu-96, the target phosphate and three water molecules. This observation is consistent with previously reported crystal structure of APE1 with Mg^{2+} cofactor (PDB entry 2ISI; R. Agarwal, unpublished data). The observed location suggests that the Mg^{2+} ion performs at least two functions. The first one is to keep the abasic site everted from the double helix by interacting with DNA binding domain of APE1. The second function is to coordinate the O atoms of the 5′-phosphate during catalysis, and rearrange the electron density in order to facilitate hydrolysis of the phosphodiester bond. During the formation of the catalytic complex, the side chain of Asn-212 forms a hydrogen bond with the 5′ O atom of the F site. The Asp-210 carboxylate binds a water molecule that in turn coordinates the 5′-phosphate of the abasic site. At the same time, the N1 atom of His-309, which is located at a distance of 3.8 Å from the target phosphate, most likely coordinates the substrate via a hydrogen bond. Therefore, our dynamic simulations show that the target site of the DNA substrate is securely fixed in the WT APE1 active site via non-covalent interactions with specific amino acids and the Mg^{2+} ion, which acts as a “clip” between the enzyme and DNA.

Analysis of MD trajectories for N212D and N212A APE1 indicated a large distortion of the active site geometry for both mutants. Fig. 6B shows the position of the F site and the key amino acids in the N212D mutant in comparison with WT APE1. It was found that Asn→Asp substitution resulted in disruption of the hydrogen bond between Asn-212 and the 5′ O atom of abasic sugar. Without this coordination, the F site would move back into the DNA helix from the active site of the mutant. Indeed, in the final structure of N212D–substrate complex the 5′ O atom and the target P–O bond were shifted by 1.2 Å and 1.9 Å compared to WT APE1. Importantly, the coordination of Mg^{2+} in the complex of N212D APE1 with F(2-aPu) substrate was significantly disturbed. The distance between the coordinating carboxylate group of Glu-96 and the metal ion increased by 1.6 Å as compared to its position in WT APE1. At the same time, there could be an alternative hydrogen bond between the carboxylate moiety of Asp-212 and the charged atoms at the

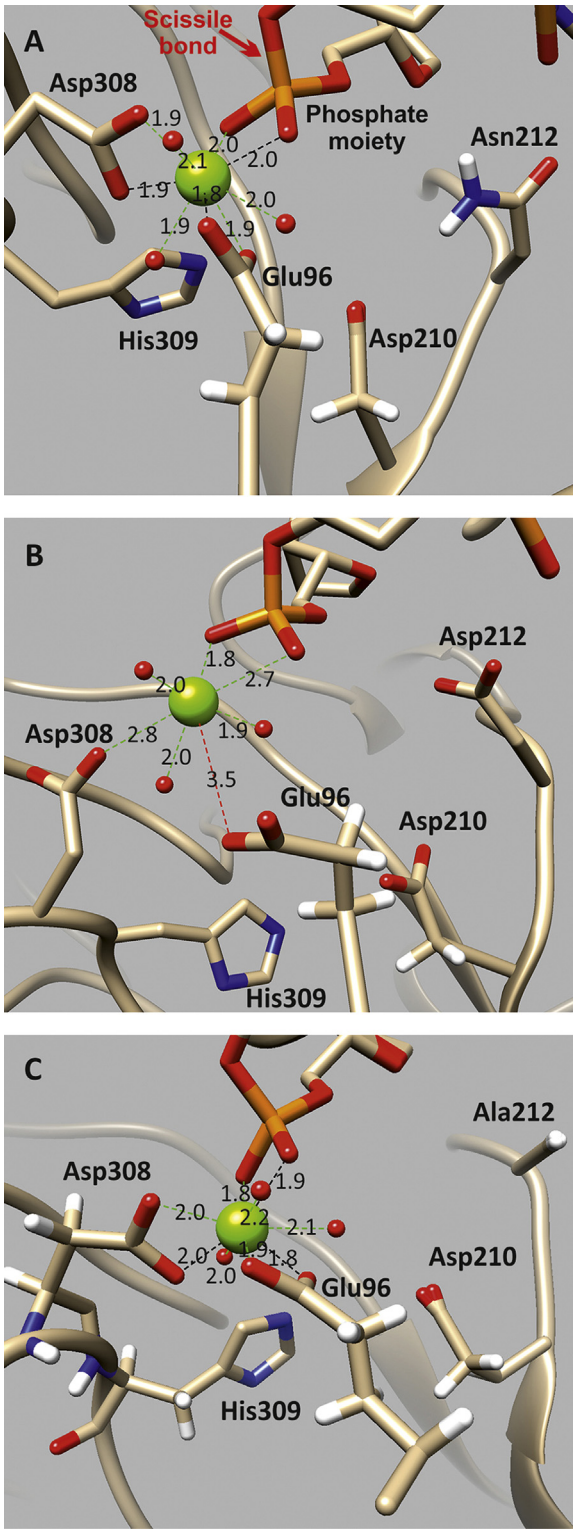

Fig. 6. Snapshots of MD simulations of wild type (A), N212D (B) and N212A (C) APE1 complexed with F(2-aPu) substrate. The coordination of magnesium ion (green sphere) in aqua complex (red sphere) is shown. In all structures the Mg^{2+} ion is coordinated by two carboxylate groups of Glu-96 and Asp-308, the 5′-phosphate moiety and three water molecules. The metal ion moved together with coordinating groups throughout the MD trajectory. The distances between Mg^{2+} and coordinating atoms are presented as dashed lines. Glu-96, Asp-210, Asn-212, Asp-212, Ala-212, Asp-308 and His-309 as well as DNA phosphate moiety are shown in the stick model coloured according to the atom type (*khaki*, carbons; *blue*, nitrogens; *red*, oxygens; *white*, hydrogens; *brown*, phosphorus atoms). The rest of the protein is shown as a semitransparent schematic model. (For interpretation of the references to colour in this figure legend, the reader is referred to the web version of the article.)

abasic site region of the DNA helix, promoting catalytically active complex formation. The most pronounced difference was observed in the side chain position of His-309. When Asn-212 is substituted by Asp, the imidazole ring of His-309 is rotated around the C^{α}-C^{β} bond, resulting in an increase in the distance between the N1 atom and the DNA target phosphate from 3.8 Å to 9.4 Å. As known from literature, His-309 and Glu-96 are essential catalytic residues responsible for correct location of abasic ribose in the APE1 active site [10,11]. The observed changes most likely give rise to a decrease in the N212D APE1 catalysis rate, but do not preclude completion of substrate cleavage. Thus, our MD results are in good agreement with pre-steady-state kinetics data.

MD simulations of the N212A-F(2-aPu) substrate complex also revealed substantial changes in the arrangement of the amino acids within the active site (Fig. 6C), albeit different from the N212D mutant. The main distinction is that N212A APE1 could not generate the hydrogen bonding network between Ala-212, Asp-210, and catalytic water, thereby impeding incision of the substrate. The imidazole ring of His-309 was substantially shifted away from the target bond, and it restricted its participation in catalysis. These changes most likely lead to the inhibition of N212A catalytic activity. It is interesting that coordination of the Mg^{2+} ion within the N212A APE1 active site matches its coordination in WT APE1. In particular, the Glu-96 and Asp-308 residues located within 1.9 Å and 2.0 Å from the metal ion, satisfying the coordination geometry of WT APE1. Therefore, one can propose that coordination of the metal ion play less important role at the substrate incision step. On the other hand, substitution of the bulky Asn-212 residue with a compact alanine enlarges the active site pocket of APE1 from 3.1 to 5.6 Å, which may facilitate recognition and binding of abasic DNA. This assumption correlates with the biochemical results obtained for N212A APE1, which demonstrated a rapid specific binding to DNA substrate and formation of the pre-catalytic complex, in contrast to N212D APE1.

Stopped-flow Trp fluorescence traces, obtained from interactions of N212A APE1 with specific substrates, had larger amplitudes compared to those of N212D APE1. This experimental fact can be explained using MD simulation. Indeed, one of the APE1 Trp residues is located in the active site adjacent to the bound abasic site. As mentioned above, the extended active site pocket characterizes the N212A structure, providing the Trp-280 side chain with a more hydrophilic environment that can result in increased contribution of Trp-280 to total enzyme fluorescence.

4. Discussion

Asn-212 plays a key role in the catalytic mechanism of human APE1. Mutation of this residue resulted in the inhibition of enzyme activity [11,12]. A combined bioinformatics screening of important SNPs in the APE1 gene has demonstrated that mutations N212K and N212H are intolerant, and likely to disrupt the functional site of APE1 [14]. In the light of these data, it was important to ascertain the effect of Asn-212 substitutions on particular steps of the APE1 catalytic mechanism. In the current study, we applied site-directed mutagenesis combined with pre-steady-state kinetic analysis and MD simulations in order to identify and quantitatively describe specific reaction steps disrupted by Asn-212 modifications. Aspartate and alanine were chosen to substitute Asn-212; the first contains a carboxylate terminal group instead of the amide, while the second has no polar side chain. Individual reaction steps were detected by the stopped-flow method using the intrinsic fluorescence of mutant enzymes, as well as the fluorescence of the 2-aPu base introduced into DNA substrates. To evaluate the mechanism and kinetic parameters of abasic DNA cleavage by the mutant proteins, we studied interactions of N212D and N212A APE1 with short double-stranded

ODNs, under single turnover conditions. The ODNs used contained either the natural AP site or F. It was found that both mutants and substrates change their conformation during the course of catalysis. It was important that the individual reaction steps observed by Trp and 2-aPu fluorescence coincided with each other, indicating that the enzyme and its substrate undergo concerted conformational changes during the catalytic cycle. The four-step reaction mechanism and rate constants of individual steps were determined by a non-linear regression analysis. The results showed that both mutants bind specifically to AP- or F-containing substrates in order to establish the intermediate complex, (ES)′, and are transformed into the enzyme–product complex at the next reaction step. However, the efficiency of binding and incision differs depending on Asn-212 substitution and the DNA substrate type. The affinity, in terms of the association constant, K_a, of both mutant proteins to the stable F analogue is 2.5–3-fold higher than to the natural AP site, consistent with previously published K_a values for WT APE1 [15]. The interesting outcome of the pre-steady-state kinetic analysis is that the N212A mutant binds AP substrate three times faster and more efficiently compared to N212D APE1, despite the absence of the polar side chain in its active site. When compared to WT APE1, the relative affinity of N212A and N212D mutants to the natural AP site is reduced by 16 and 60 times, respectively ($K_a^{WT} > K_a^{N212A} > K_a^{N212D}$). As demonstrated by our MD simulations, when Asp is substituted for Asn-212, the hydrogen bonding network between Asp-212, Asp-210 and the catalytic water molecule is most probably maintained. At the same time, coordination of the Mg^{2+} is significantly disturbed due to dislocation of Glu-96 residue by 1.6 Å relative to its position in the WT APE1 (Fig. 6B). These changes probably disrupt the formation of the specific intermediate complex (ES)′ between the N212D mutant and abasic DNA. N212A APE1, in turn, retains the proper orientation of the metal ion (Fig. 6C), but lacks the polar side chain of Asn-212. Based on the findings we consider that one reason for the rapid formation of (ES)′ complex in the case of N212A APE1 results from an extension of the active site pocket, facilitating substrate accessibility. Another important factor responsible for formation of the specific complex between APE1 and abasic DNA is proper coordination of Mg^{2+} by carboxylate moieties, water molecules and 5′ phosphate group.

As expected, our stopped-flow and chemical quenching results indicate a significant decrease in the cleavage rate for both mutants. When Asp substitutes Asn-212, the conformational transition corresponding to the catalytic incision step occurs in between 40 and 1000 s instead of 0.2–2 s as with WT APE1. The rate of phosphodiester bond hydrolysis in terms of the irreversible incision constant, k_3, is suppressed by ~550-fold. Yet PAGE analysis shows that the reaction product is still formed, albeit taking between 20 and 30 min in the case of the natural AP site, and 150–200 min in the case of F. Taking structural considerations into account, we believe that N212D APE1 retains the ability to orient the target DNA 5′-phosphate in more or less the correct position for nucleophile attack with Asp-212, Asp-210, and the catalytic water molecule. In the case of Asn→Ala substitution, the endonuclease activity of APE1 is almost terminated. In fact, after two relatively fast binding steps, stopped-flow fluorescence traces demonstrated the slow conformational transitions, which cannot be fitted by global analysis. Using the chemical quench assay, we detected a low activity level of the N212A mutant against the AP and F substrates, with observed incision rates of 4.4×10^{-5} s^{-1} and 1.4×10^{-5} s^{-1}, respectively. This indicates an ~70,000–100,000-fold decrease in the rate of the 12 bp abasic DNA cleavage compared to WT enzyme. Our MD simulations have revealed dramatic changes in the N212A mutant structure, which generally correlate with N212D active site changes. The major difference between mutant structures is the absence of non-covalent interactions between Asn-212, Asp-210, the target 5′-phosphate, and catalytic water in the case of N212A APE1. Therefore, we assume this difference to be the reason for the impaired incision activity. This conclusion agrees well with the findings from the new crystal structures of APE1 on its own, and when it is complexed to product DNA [10,11].

This study provides the first MD simulation of the APE1 complex with the F(2-aPu) substrate, where the 2-aPu fluorescent base is located 3′ to the F damage. Fluorescent properties of this adenine analogue are widely used for studying DNA-dependent enzymes [38–40]. Changes in the 2-aPu fluorescence intensity during enzyme–substrate interactions reflect the dynamic behaviour of DNA substrates and products. Our previous study included MD simulations of abasic DNA duplex structures containing 2-aPu in various positions around the abasic site [16]. It was found that DNA substrates containing the 2-aPu base 3′ to the abasic site generally retain a B-like geometry, while individual nucleotides of the abasic site region demonstrate a high degree of internal flexibility. In the framework of the present study, it was interesting to consider an orientation of 2-aPu as a part of the DNA substrate bound to the APE1 active site. As a result, we found that the 3′ 2-aPu base is rather movable throughout the simulation process. Thus, its location is useful for observing DNA conformational transitions for two reasons: first, the 2-aPu residue lies close to the abasic site void, indicating that the fluorescence intensity changes correspond to conformational transitions of the enzyme–substrate complex. Second, positioning of the abnormal base 3′ to the damage does not affect the incision of the 5′-phosphate of the AP site. Therefore, it seems likely that our stopped-flow 2-aPu fluorescence traces faithfully reflect conformational transitions of the substrate molecule occurring during binding and specific cleavage by the APE1 protein. These findings may be helpful to design new 2-aPu-labelled DNA substrates.

In conclusion, this study establishes the specific impact of Asn-212 on binding and catalytic activity of the human AP endonuclease APE1. The pre-steady-state kinetic analysis, in combination with MD simulations, allows us to study the role of Asn-212 in particular steps of the reaction mechanism in detail. Our data indicate that mutating Asn-212 to Ala dramatically decreases the rate of the incision step, but maintains the ability of APE1 to recognize and bind specifically to abasic DNA, albeit less efficiently than WT APE1. In contrast, N212D APE1 possesses a weakened ability to specifically bind the DNA substrate within the pre-catalytic complex, but can successfully incise the damaged DNA. Using MD simulations, we have shown that the large distortion of the active site geometry takes place in both mutants, resulting in the dislocation of key amino acid residues. The substitution of Ala for Asn-212 leads to the disruption of the hydrogen bonding network between Asn-212, Asp-210, and catalytic water, whereas the Asp substitution disturbs significantly the metal ion coordination. The data obtained support the recently proposed hypothesis that the water molecule coordinated by Asn-212 and Asp-210 can serve as the nucleophile for hydrolysis of the target phosphodiester bond [10,11]. Thus, our data have identified the role of the conserved Asn-212 residue in realization of catalytic activity of human APE1, and illustrate its significance in the formation of the catalytically competent conformation.

Conflict of interest statement

The authors declare that there are no conflicts of interest.

Acknowledgements

We thank Mrs. Tatiana Bushueva for the synthesis of oligodeoxyribonucleotides.

This work was supported in part by grants from MCB Programme of RAS (No 6.11), the Russian Foundation for Basic Research Grants 13-04-00013 (OSF), 14-04-00806 (VVK) and 14-04-31448 (LYK), the Russian Ministry of Education and Science (SS-1205.2014.4 and NSU-SB RAS Collaborative Lab).

Appendix A. Supplementary data

Supplementary data associated with this article can be found, in the online version, at http://dx.doi.org/10.1016/j.dnarep.2014.06.008.

References

[1] T. Lindahl, Suppression of spontaneous mutagenesis in human cells by DNA base excision-repair, Mutat. Res. 462 (2000) 129–135.
[2] B. Demple, J.S. Sung, Molecular and biological roles of Ape1 protein in mammalian base excision repair, DNA Repair (Amst) 4 (2005) 1442–1449.
[3] T.A. Winters, W.D. Henner, P.S. Russell, A. McCullough, T.J. Jorgensen, Removal of 3′-phosphoglycolate from DNA strand-break damage in an oligonucleotide substrate by recombinant human apurinic/apyrimidinic endonuclease 1, Nucleic Acids Res. 22 (1994) 1866–1873.
[4] D.M. Wilson 3rd, Properties of and substrate determinants for the exonuclease activity of human apurinic endonuclease Ape1, J. Mol. Biol. 330 (2003) 1027–1037.
[5] F.C. Bernstein, T.F. Koetzle, G.J. Williams, E.F. Meyer Jr., M.D. Brice, J.R. Rodgers, O. Kennard, T. Shimanouchi, M. Tasumi, The Protein Data Bank: a computer-based archival file for macromolecular structures, J. Mol. Biol. 112 (1977) 535–542.
[6] C.D. Mol, T. Izumi, S. Mitra, J.A. Tainer, DNA-bound structures and mutants reveal abasic DNA binding by APE1 and DNA repair coordination, Nature 403 (2000) 451–456.
[7] T. Izumi, C.H. Schein, N. Oezguen, Y. Feng, W. Braun, Effects of backbone contacts 3′ to the abasic site on the cleavage and the product binding by human apurinic/apyrimidinic endonuclease (APE1), Biochemistry 43 (2004) 684–689.
[8] P.T. Beernink, B.W. Segelke, M.Z. Hadi, J.P. Erzberger, D.M. Wilson 3rd, B., Two divalent metal ions in the active site of a new crystal form of human apurinic/apyrimidinic endonuclease, Ape1: implications for the catalytic mechanism Rupp, J. Mol. Biol. 307 (2001) 1023–1034.
[9] N. Oezguen, C.H. Schein, S.R. Peddi, T.D. Power, T. Izumi, W. Braun, A moving metal mechanism for substrate cleavage by the DNA repair endonuclease APE-1, Proteins 68 (2007) 313–323.
[10] B.A. Manvilla, E. Pozharski, E.A. Toth, A.C. Drohat, Structure of human apurinic/apyrimidinic endonuclease 1 with the essential Mg^{2+} cofactor, Acta Crystallogr. D Biol. Crystallogr. 69 (2013) 2555–2562.
[11] S.E. Tsutakawa, D.S. Shin, C.D. Mol, T. Izumi, A.S. Arvai, A.K. Mantha, B. Szczesny, I.N. Ivanov, D.J. Hosfield, B. Maiti, M.E. Pique, K.A. Frankel, K. Hitomi, R.P. Cunningham, S. Mitra, J.A. Tainer, Conserved structural chemistry for incision activity in structurally non-homologous apurinic/apyrimidinic endonuclease APE1 and endonuclease IV DNA repair enzymes, J. Biol. Chem. 288 (2013) 8445–8455.
[12] D.G. Rothwell, I.D. Hickson, Asparagine 212 is essential for abasic site recognition by the human DNA repair endonuclease HAP1, Nucleic Acids Res. 24 (1996) 4217–4221.
[13] P.J. Luncsford, B.A. Manvilla, D.N. Patterson, S.S. Malik, J. Jin, B.J. Hwang, R. Gunther, S. Kalvakolanu, L.J. Lipinski, W. Yuan, W. Lu, A.C. Drohat, A.L. Lu, E.A. Toth, Coordination of MYH DNA glycosylase and APE1 endonuclease activities via physical interactions, DNA Repair (Amst) 12 (2013) 1043–1052.
[14] E.T. Yu, M.Z. Hadi, Bioinformatic processing to identify single nucleotide polymorphism that potentially affect Ape1 function, Mutat. Res. 722 (2011) 140–146.
[15] L.Y. Kanazhevskaya, V.V. Koval, D.O. Zharkov, P.R. Strauss, O.S. Fedorova, Conformational transitions in human AP endonuclease 1 and its active site mutant during abasic site repair, Biochemistry 49 (2010) 6451–6461.
[16] L.Y. Kanazhevskaya, V.V. Koval, Y.N. Vorobjev, O.S. Fedorova, Conformational dynamics of abasic DNA upon interactions with AP endonuclease 1 revealed by stopped-flow fluorescence analysis, Biochemistry 51 (2012) 1306–1321.
[17] N.A. Timofeyeva, V.V. Koval, A.A. Ishchenko, M.K. Saparbaev, O.S. Fedorova, Lys98 substitution in human AP endonuclease 1 affects the kinetic mechanism of enzyme action in base excision and nucleotide incision repair pathways, PLoS One 6 (2011).
[18] K.J. Breslauer, R. Frank, H. Blocker, L.A. Marky, Predicting DNA duplex stability from the base sequence, Proc. Natl. Acad. Sci. U. S. A. 83 (1986) 3746–3750.
[19] N. Sugimoto, S. Nakano, M. Yoneyama, K. Honda, Improved thermodynamic parameters and helix initiation factor to predict stability of DNA duplexes, Nucleic Acids Res. 24 (1996) 4501–4505.
[20] C.A. Gelfand, G.E. Plum, A.P. Grollman, F. Johnson, K.J. Breslauer, Thermodynamic consequences of an abasic lesion in duplex DNA are strongly dependent on base sequence, Biochemistry 37 (1998) 7321–7327.
[21] O.S. Fedorova, G.A. Nevinsky, V.V. Koval, A.A. Ishchenko, N.L. Vasilenko, K.T. Douglas, Stopped-flow kinetic studies of the interaction between *Escherichia coli* Fpg protein and DNA substrates, Biochemistry 41 (2002) 1520–1528.
[22] N.A. Kuznetsov, V.V. Koval, D.O. Zharkov, Y.N. Vorobjev, G.A. Nevinsky, K.T. Douglas, O.S. Fedorova, Pre-steady-state kinetic study of substrate specificity of *Escherichia coli* formamidopyrimidine–DNA glycosylase, Biochemistry 46 (2007) 424–435.
[23] P. Kuzmic, Program DYNAFIT for the analysis of enzyme kinetic data: application to HIV proteinase, Anal. Biochem. 237 (1996) 260–273.
[24] M.M. Harding, Geometry of metal–ligand interactions in proteins, Acta Crystallogr. D Biol. Crystallogr. 57 (2001) 401–411.
[25] R. Salomon-Ferrer, D.A. Case, R.C. Walker, An overview of the Amber biomolecular simulation package, Wires Comput. Mol. Sci. 3 (2013) 198–210.
[26] D.A. Case, T.A. Darden, I. Cheatham, T. E., C.L. Simmerling, J. Wang, R.E. Duke, R. Luo, R.C. Walker, W. Zhang, K.M. Merz, B. Roberts, S. Hayik, A. Roitberg, G. Seabra, J. Swails, A.W. Götz, I. Kolossváry, K.F. Wong, F. Paesani, J. Vanicek, R.M. Wolf, J. Liu, X. Wu, S.R. Brozell, T. Steinbrecher, H. Gohlke, Q. Cai, X. Ye, J. Wang, M.-J. Hsieh, G. Cui, D.R. Roe, D.H. Mathews, M.G. Seetin, R. Salomon-Ferrer, C. Sagui, V. Babin, T. Luchko, S. Gusarov, A. Kovalenko, K.P. A., AMBER 12, University of California, San Francisco, 2012.
[27] u.d. D. A.Case, the database is maintained by Dr. Richard Bryce, (http://www.pharmacy.manchester.ac.uk/bryce/amber#nuc).
[28] A.W. Gotz, M.J. Williamson, D. Xu, D. Poole, S. Le Grand, R.C. Walker, Routine microsecond molecular dynamics simulations with AMBER on GPUs. 1. Generalized born, J. Chem. Theory Comput. 8 (2012) 1542–1555.
[29] A.W.G.R. Salomon-Ferrer, D. Poole, S. Le Grand, R.C. Walker, Routine microsecond molecular dynamics simulations with AMBER on GPUs. 2. Explicit solvent particle mesh Ewald, J. Chem. Theory Comput. 9 (2013) 3878–3888.
[30] E.F. Pettersen, T.D. Goddard, C.C. Huang, G.S. Couch, D.M. Greenblatt, E.C. Meng, T.E. Ferrin, UCSF chimera – A visualization system for exploratory research and analysis, J. Comput. Chem. 25 (2004) 1605–1612.
[31] P.R. Strauss, W.A. Beard, T.A. Patterson, S.H. Wilson, Substrate binding by human apurinic/apyrimidinic endonuclease indicates a Briggs-Haldane mechanism, J. Biol. Chem. 272 (1997) 1302–1307.
[32] Y. Masuda, R.A. Bennett, B. Demple, Dynamics of the interaction of human apurinic endonuclease (Ape1) with its substrate and product, J. Biol. Chem. 273 (1998) 30352–30359.
[33] Y. Masuda, R.A. Bennett, B. Demple, Rapid dissociation of human apurinic endonuclease (Ape1) from incised DNA induced by magnesium, J. Biol. Chem. 273 (1998) 30360–30365.
[34] R.L. Maher, L.B. Bloom, Pre-steady-state kinetic characterization of the AP endonuclease activity of human AP endonuclease 1, J. Biol. Chem. 282 (2007) 30577–30585.
[35] N.A. Timofeyeva, V.V. Koval, D.G. Knorre, D.O. Zharkov, M.K. Saparbaev, A.A. Ishchenko, O.S. Fedorova, Conformational dynamics of human AP endonuclease in base excision and nucleotide incision repair pathways, J. Biomol. Struct. Dyn. 26 (2009) 637–652.
[36] D.M. Wilson 3rd, M. Takeshita, A.P. Grollman, B. Demple, Incision activity of human apurinic endonuclease (Ape) at abasic site analogs in DNA, J. Biol. Chem. 270 (1995) 16002–16007.
[37] P.A. Fagan, C. Fabrega, R. Eritja, M.F. Goodman, D.E. Wemmer, NMR study of the conformation of the 2-aminopurine:cytosine mismatch in DNA, Biochemistry 35 (1996) 4026–4033.
[38] C.A. Dunlap, M.D. Tsai, Use of 2-aminopurine and tryptophan fluorescence as probes in kinetic analyses of DNA polymerase beta, Biochemistry 41 (2002) 11226–11235.
[39] E.S. Dyakonova, V.V. Koval, A.A. Ishchenko, M.K. Saparbaev, R. Kaptein, O.S. Fedorova, Kinetic mechanism of the interaction of *Saccharomyces cerevisiae* AP-endonuclease 1 with DNA substrates, Biochemistry (Mosc) 77 (2012) 1162–1171.
[40] A. Sharma, C. Doucette, F.N. Biro, M.M. Hingorani, Slow conformational changes in MutS and DNA direct ordered transitions between mismatch search, recognition and signaling of DNA repair, J. Mol. Biol. 425 (2013) 4192–4205.